2014

Magnetization curves of sintered heavy tungsten alloys for applications in MRI-guided radiotherapy

Stefan Kolling
University of Sydney

Bradley Oborn
University of Wollongong, boborn@uow.edu.au

Paul Keall
University of Sydney

Josip Horvat
University of Wollongong, jhorvat@uow.edu.au

Publication Details

Kolling, S., Oborn, B. M., Keall, P. J. & Horvat, J. (2014). Magnetization curves of sintered heavy tungsten alloys for applications in MRI-guided radiotherapy. Medical Physics, 41 (6), 061707-1-061707-6.

Magnetization curves of sintered heavy tungsten alloys for applications in MRI-guided radiotherapy

Abstract
Purpose: Due to the current interest in MRI-guided radiotherapy, the magnetic properties of the materials commonly used in radiotherapy are becoming increasingly important. In this paper, mea- surement results for the magnetization (BH) curves of a range of sintered heavy tungsten alloys used in radiation shielding and collimation are presented.

Methods: Sintered heavy tungsten alloys typically contain > 90% tungsten and < 10% of a combina- tion of iron, nickel, and copper binders. Samples of eight different grades of sintered heavy tungsten alloys with varying binder content were investigated. Using a superconducting quantum interference detector magnetometer, the induced magnetic moment m was measured for each sample as a function of applied external field $H_0$and the BH curve derived.

Results: The iron content of the alloys was found to play a dominant role, directly influencing the magnetization M and thus the nonlinearity of the BH curve. Generally, the saturation magnetization increased with increasing iron content of the alloy. Furthermore, no measurable magnetization was found for all alloys without iron content, despite containing up to 6% of nickel. For two samples from different manufacturers but with identical quoted nominal elemental composition (95% W, 3.5% Ni, 1.5% Fe), a relative difference in the magnetization of 11%–16% was measured.

Conclusions: The measured curves show that the magnetic properties of sintered heavy tungsten alloys strongly depend on the iron content, whereas the addition of nickel in the absence of iron led to no measurable effect. Since a difference in the BH curves for two samples with identical quoted nominal composition from different manufacturers was observed, measuring of the BH curve for each individual batch of heavy tungsten alloys is advisable whenever accurate knowledge of the magnetic properties is crucial. The obtained BH curves can be used in FEM simulations to predict the magnetic impact of sintered heavy tungsten alloys.

Keywords
magnetization, sintered, mri, curves, guided, heavy, applications, alloys, tungsten, radiotherapy

Disciplines
Engineering | Science and Technology Studies

Publication Details
Kolling, S., Oborn, B. M., Keall, P. J. & Horvat, J. (2014). Magnetization curves of sintered heavy tungsten alloys for applications in MRI-guided radiotherapy. Medical Physics, 41 (6), 061707-1-061707-6.

Magnetization curves of sintered heavy tungsten alloys for applications in MRI-guided radiotherapy

Stefan Kolling

Sydney Medical School, University of Sydney, NSW 2006, Australia

Joseph Horvat

Institute for Superconducting and Electronic Materials, University of Wollongong, Wollongong, NSW 2500, Australia and School of Physics, University of Wollongong, Wollongong, NSW 2500, Australia

Bradley M Oborn

Illawarra Cancer Care Centre (ICCC), Wollongong, NSW 2500, Australia and Centre for Medical Radiation Physics (CMRP), University of Wollongong, Wollongong, NSW 2500, Australia

Paul J Keall*

Sydney Medical School, University of Sydney, NSW 2006, Australia and Ingham Institute for Applied Medical Research, Liverpool NSW 2170

(Dated: March 19, 2014)

Abstract

Purpose: Due to the current interest in MRI-guided radiotherapy, the magnetic properties of the materials commonly used in radiotherapy are becoming increasingly important. In this note, measurement results for the magnetization (BH) curves of a range of sintered heavy tungsten alloys used in radiation shielding and collimation are presented.

Methods: Sintered heavy tungsten alloys typically contain $> 90\,\%$ tungsten and $< 10\,\%$ of a combination of iron, nickel and copper binders. Samples of 8 different grades of sintered heavy tungsten alloys with varying binder content were investigated. Using a Superconducting Quantum Interference Detector (SQUID) magnetometer, the induced magnetic moment m was measured for each sample as a function of applied external field H_0 and the BH curve derived.

Results: The iron content of the alloys was found to play a dominant role, directly influencing the magnetization M and thus the nonlinearity of the BH curve. Generally, the saturation magnetization increased with increasing iron content of the alloy. Furthermore, no measurable magnetization was found for all alloys without iron content, despite containing up to 6% of nickel. For two samples from different manufacturers but with identical quoted nominal elemental composition (95 % W, 3.5 % Ni, 1.5 % Fe), a relative difference in the magnetization of $9 - 15\,\%$ was measured.

Conclusions: The measured curves show that the magnetic properties of sintered heavy tungsten alloys strongly depend on the iron content, whereas the addition of nickel in the absence of iron led to no measurable effect. Since a difference in the BH curves for two samples with identical quoted nominal composition from different manufacturers was observed, measuring of the BH curve for each individual batch of heavy tungsten alloys is advisable whenever accurate knowledge of the magnetic properties is crucial. The obtained BH curves can be used in FEM simulations to predict the magnetic impact of sintered heavy tungsten alloys.

Key words: magnetization curve, sintered heavy tungsten alloy, radiation shielding, magnetic fields

* Author to whom correspondence should be addressed. E-mail: paul.keall@sydney.edu.au

I. INTRODUCTION

In recent years, the development of new modalities utilising the strengths of MRI devices for the benefit of better radiotherapy treatment has gained substantial interest. Active research in the field of MRI-guided radiotherapy is currently underway, with the first prototypes already constructed[1–3]. In this process, one major challenge to overcome is the magnetic interference between the MRI device and the hardware components of the radiotherapy treatment system which, historically, were not designed to be operated in a magnetic field. Hence, a characterisation of the magnetic properties of the materials used is essential, i.e. their magnetization or BH curves need to be known in order to predict the magnetic impact. While this information can be readily found in the literature for standard ferromagnetic materials, such as iron, nickel and common alloys of these, there is no publicly available data for the BH curves of so-called sintered heavy tungsten alloys. These alloys typically contain $> 90\,\%$ tungsten (by weight); the remaining $< 10\,\%$ are made up by copper, iron and nickel which serve as a binder matrix to increase ductility and machinability[4]. Due to their unique combination of high density, mechanical strength, good machinability and non-toxicity[5], they are widely used for radiation shielding and collimation purposes (e.g. in MLC's). In this note, the magnetization curves of eight grades of commercially available sintered heavy tungsten alloys have been determined experimentally with a SQUID magnetometer.

II. METHODS AND MATERIALS

A. Sintered heavy tungsten alloy samples

Table I lists the eight samples of sintered heavy tungsten alloys the magnetization curves of which were experimentally determined. The samples were provided by the two distributors Midwest Tungsten Service[6] and Wolfmet[7]. The selected grades differed in elemental composition, with an iron content varying from $3\,\%$ down to $0\,\%$. The three iron-free samples contained between $6\,\%$ and $3.5\,\%$ of the relatively less-ferromagnetic nickel. The F_xN_x sample was cut from a decommissioned Varian Millennium 120 MLC leaf. Although the exact elemental composition was unknown, obtaining the BH curve of this sample was of particular interest due to its widespread use in MLC's. The two samples referred to as

TABLE I. List of sintered heavy tungsten alloy samples examined in this study. Grades marked with [1] or [2] were provided by Midwest Tungsten Service[6] or Wolfmet[7], respectively.

Sample	**Elem. composition (wt%)**				**Grade**
	W	Fe	Ni	Cu	
F_xN_x	–	–	–	–	MLC
$F_{3.0}N_{7.0}$	90.0	3.0	7.0	0.0	MT17F[1]
$F_{1.5}N_{3.5}$	95.0	1.5	3.5	0.0	MT18F[1]
$F_{1.5}N'_{3.5}$	95.0	1.5	3.5	0.0	HE395[2]
$F_{0.9}N_{2.1}$	97.0	0.9	2.1	0.0	MT185[1]
$F_{0.0}N_{6.0}$	90.0	0.0	6.0	4.0	MT17C[1]
$F_{0.0}N_{4.0}$	95.0	0.0	4.0	1.0	HA195[2]
$F_{0.0}N_{3.5}$	95.0	0.0	3.5	1.5	MT18C[1]

$F_{1.5}N_{3.5}$ and $F_{1.5}N'_{3.5}$ were quoted with identical nominal composition, but were produced by different manufacturers. Comparing the results for these samples will indicate if knowledge of the nominal elemental composition (as quoted by the manufacturer) is sufficient to predict the magnetization curve of a sample with respect to a measured reference curve with the same quoted nominal composition. In preparation for the experiments, the samples were cut into cubic blocks of $3 \times 3 \times 3\,\mathrm{mm}^3$ to fit into the loader cup of the measurement device.

B. Measurement of magnetic moment

A SQUID magnetometer (Magnetic Property Measurement System 5XL, Quantum Design) was used to determine the magnetic moment m of the sintered heavy tungsten alloy samples. The measurements were carried out at a temperature of 300 K. Starting from a fully demagnetized sample, the magnetometer measured the magnetic moment m induced in the sample of the sintered heavy tungsten alloy as a function of applied external field H_0 in the range of 0 to 8×10^5 A/m. Data points were acquired with a step width of 6×10^3 A/m in the low-field range from 0 to 90×10^3 A/m; the step width was increased to 40×10^3 A/m and 80×10^3 A/m above 90×10^3 A/m and 240×10^3 A/m, respectively. The magnetization curve of the MLC-leaf sample had already been determined in a related research project where

the step widths in the measurement sequence were slightly different[8]. Since sampling the magnetization curves with the exact same point density was not necessary for this work, the previously obtained data was used (see Table II in the supplemental data).

C. Data analysis

The magnetic moment m was normalized by the sample volume, yielding the volume-independent magnetization M. In materials of finite length, magnetic poles are generated near the ends of the sample which gives rise to a demagnetizing field H_d opposing the applied field H_0[9]:

$$H_d = N_d M, \tag{1}$$

where the constant of proportionality N_d is called demagnetizing factor. For the demagnetizing factor, the approximate expression $N_d = 1/(2n+1)$ for a uniformly magnetized rectangular rod was used[10]. The dimensional ratio n was 1 for our cubic samples. Subtraction of the demagnetizing field H_d from the applied field H_0 yields the internal field

$$H = H_0 - H_d. \tag{2}$$

Then, the magnetic flux density B was derived according to the fundamental relation

$$B(H) = \mu_0(H + M), \tag{3}$$

where μ_0 is the vacuum permeability[9].

D. Error analysis

The SQUID magnetometer provides the values for the applied magnetic field with a relative accuracy of $\frac{\sigma_H}{H} = 10^{-7}$. Furthermore, the relative sensitivity for the measurement of the magnetic moment is quoted by the manufacturer as $\frac{\sigma_m}{m} = 10^{-4}$[11]. The samples were cut into cubic blocks with 3.00 mm edge length by the University of Wollongong workshop with an accuracy of ± 0.05 mm. In order to reduce the measurement uncertainty, the dimensions of each tungsten sample have been measured with calipers to an uncertainty in the edge

lengths l of $\sigma_l = 0.01\,\mathrm{mm}$. Hence, the uncertainties in the magnetisation M and magnetic flux density B could be derived as

$$\sigma_M = \sqrt{\left(\frac{\partial M}{\partial l}\sigma_l\right)^2 + \left(\frac{\partial M}{\partial m}\sigma_m\right)^2} \approx \frac{\partial M}{\partial l}\sigma_l = 0.01M \tag{4}$$

and

$$\sigma_B = \sqrt{\left(\frac{\partial B}{\partial M}\sigma_M\right)^2 + \left(\frac{\partial B}{\partial H}\sigma_H\right)^2} \approx \frac{\partial B}{\partial M}\sigma_M = 0.01\mu_0 M, \tag{5}$$

where the two neglected terms associated with σ_m and σ_H were more than 10^2 times smaller compared to the dominant terms associated with σ_l and σ_M, respectively. Essentially, the accuracy of the experimental data is limited by the uncertainty in the edge lengths.

III. RESULTS AND DISCUSSION

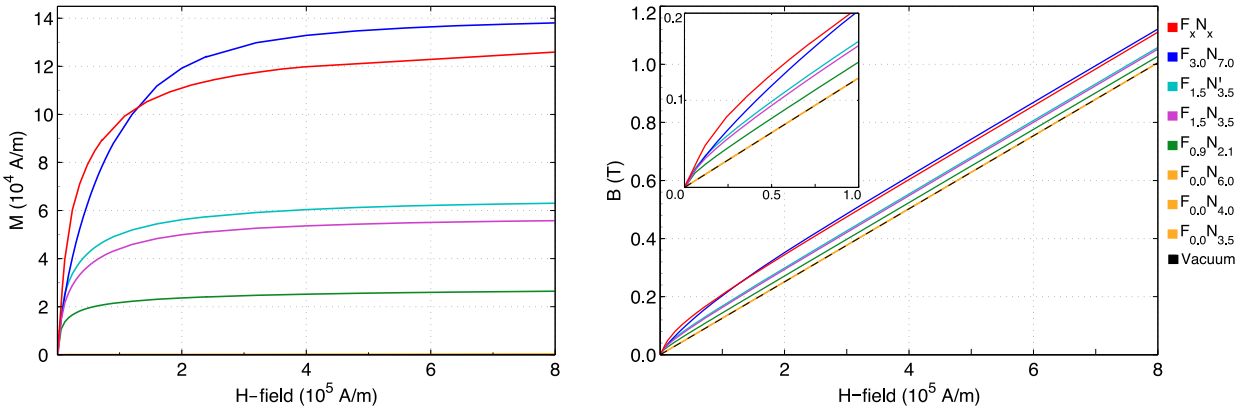

(a) M(H) (b) B(H)

FIG. 1. Measured $M(H)$ and $B(H)$ curves of eight different sintered heavy tungsten alloys. The saturation magnetization increases with the iron content of the alloys. Despite up to 6 % nickel content, the samples without iron show no measurable magnetization. The $F_{1.5}N_{3.5}$ and $F_{1.5}N'_{3.5}$ samples with identical quoted nominal composition show a relative difference in the magnetization of $11 - 16\,\%$.The uncertainties in the measurement data are too small to be visualized, but are disclosed in the Supplemental Data V.

The magnetization M measured in the H-field range of $0 - 8 \times 10^5\,\mathrm{A/m}$ is shown in Fig. 1(a) and the corresponding BH curves in Fig. 1(b). As a general trend in Fig. 1(a), the magnetization $M(H)$ becomes higher as the iron content of the sintered heavy tungsten alloy increases. For instance, a maximum saturation magnetization of about $14 \times 10^4\,\mathrm{A/m}$

is reached for the $F_{3.0}N_{7.0}$ sample. The alloys with 1.5 % iron, half the iron of the $F_{3.0}N_{7.0}$ sample, saturate at around 6×10^4 A/m; the sample with 0.9 % iron at around 2.5×10^4 A/m. The sample cut from the Varian Millennium 120 MLC leaf shows the steepest initial increase of the magnetization M with H which then flattens out and crosses the $F_{3.0}N_{7.0}$ curve at $M \approx 10 \times 10^4$ A/m, before levelling off at about 13×10^4 A/m. Such a saturation magnetization, seen in the context of the curves of the other alloys, could be a sign of an iron content somewhere between 1.5 % and 3 % (probably closer to the latter value).

Independent of their respective nickel content, no measurable magnetization was found for any of the three alloys without iron, which is in agreement with the results for a measured W-Ni-Cu heavy tungsten alloy found in the literature[12]. These findings suggest that a nickel content of up to 6 % is uncritical with regards to magnetic properties and such alloys may be used in environments with magnetic fields without concern.

The two samples with identical quoted nominal elemental composition, $F_{1.5}N_{3.5}$ and $F_{1.5}N'_{3.5}$, follow a similar course, however are not in perfect agreement: A maximum relative difference in M of 16 % is observed at low H which levels off at about 11 % in the regime of magnetic saturation. This discrepancy relates to a maximum difference of 9 % in the initial section of the corresponding BH curves (Fig. 1(b)). Above magnetic saturation, B and H are linked through a linear relation with a slope of μ_0 (Eq. 3) and hence the absolute difference between the curves remains constant. The difference can be expressed through the difference in the saturation magnetizations of both samples and amounts to $\Delta B_{sat} = \mu_0 \Delta M_{sat} \approx 6\,\mathrm{mT}$. Considering an uncertainty in the magnetisation of $\sigma_M = 1\% M$(as discussed in Section II D), it can be ruled out that the observed difference in the range of $11 - 16\% M$ is a measurement artefact.

A number of factors comes to mind that could possibly explain the difference: The actual elemental compositions of the two samples could be slightly different from what is quoted since the manufacturers work to a relatively broad tolerance and some variation in the composition between batches is likely. The different sintering procedures used by the manufacturers may have an influence on the magnetic properties by affecting the size and local concentration of the magnetic ions within the alloy. In addition, the grain structure of the constituent metal particles as well as unintentional annealing following the actual sintering may also play a part. In the literature, differences in the magnetization curves for two samples with identical elemental composition (but one in as-sintered, the other in

cold-worked condition) have been reported[13] and support this claim. No further steps were undertaken to identify how big a role each of these factors plays in the examined samples as this was not within the scope of this work. However, regardless of which is the dominant factor, the observed difference makes clear that, whenever accurate knowledge of the magnetic properties is crucial, a reference BH curve for an alloy with the same quoted nominal composition may not be sufficient to predict the magnetic impact of sintered heavy tungsten alloys from other manufacturers or even another batch of the same manufacturer. Instead, BH curves should ideally be measured for each individual batch of heavy tungsten alloys in such cases.

IV. CONCLUSION

Through the measurement of the magnetization curves of eight sintered heavy tungsten alloys, it could be shown that the magnetic properties of sintered heavy tungsten alloys strongly depend on the iron content of the alloys, whereas the addition of up to 6 % of nickel in the absence of iron led to no measurable effect. Furthermore, the observed difference in the BH curves for two samples with identical nominal composition but from different manufacturers indicates that the BH curve should be measured for each individual batch of heavy tungsten alloys whenever accurate knowledge is crucial. Using these BH curves as input for FEM simulations to predict the magnetic impact of sintered heavy tungsten alloys will be a great help in the development of new MR-based imaging and treatment modalities in radiotherapy.

V. SUPPLEMENTAL DATA

See Table II below for the measurement data.

ACKNOWLEDGMENTS

We thank the Midwest Tungsten Service and Wolfmet companies for the free supply of the tungsten alloy samples used in this study. Furthermore, we gratefully acknowledge funding

TABLE II. Data of the measured BH curves.

(a)$F_{3.0}N_{7.0}$

$H\,(\frac{A}{m})$	$B \pm \sigma_B$ (mT)
0	0.00± < 0.01
5811	19.22 ± 0.35
11909	35.78 ± 0.62
17900	50.33 ± 0.82
24007	64.17 ± 1.01
29989	77.02 ± 1.17
35961	89.35 ± 1.31
42015	101.41 ± 1.44
47987	112.96 ± 1.56
53942	124.18 ± 1.67
59968	135.25 ± 1.77
65896	145.91 ± 1.87
71904	156.49 ± 1.96
77877	166.83 ± 2.04
83885	177.04 ± 2.12
89993	187.19 ± 2.20
119963	234.98 ± 2.50
159810	295.03 ± 2.79
199801	351.51 ± 2.98
239711	405.82 ± 3.10
239720	405.67 ± 3.09
319620	511.05 ± 3.24
399566	614.07 ± 3.32
479448	715.97 ± 3.36
559313	817.40 ± 3.39
639313	918.69 ± 3.42
719330	1019.81 ± 3.43
799204	1120.63 ± 3.45

(b)$F_{1.5}N_{3.5}$

$H\,(\frac{A}{m})$	$B \pm \sigma_B$ (mT)
0	0.00± < 0.01
5901	19.55 ± 0.36
11981	33.35 ± 0.55
17972	44.37 ± 0.65
24052	54.63 ± 0.73
30034	64.19 ± 0.79
36006	73.38 ± 0.84
42051	82.44 ± 0.88
48023	91.17 ± 0.92
53978	99.74 ± 0.95
60004	108.28 ± 0.98
65941	116.62 ± 1.01
71931	124.91 ± 1.03
77904	133.12 ± 1.05
83912	141.30 ± 1.07
90020	149.57 ± 1.09
119990	189.56 ± 1.16
159837	241.69 ± 1.22
199810	293.30 ± 1.26
239729	344.43 ± 1.29
239729	344.38 ± 1.29
319638	446.16 ± 1.33
399575	547.44 ± 1.35
479457	648.42 ± 1.37
559331	749.22 ± 1.38
639348	850.10 ± 1.39
719366	950.92 ± 1.40
799240	1051.50 ± 1.41

(c) $F_{1.5}N'_{3.5}$

$H\,(\frac{A}{m})$	$B \pm \sigma_B$ (mT)
0	0.00± < 0.01
5910	21.44 ± 0.42
11990	36.57 ± 0.65
17972	48.01 ± 0.77
24070	58.58 ± 0.86
30043	68.32 ± 0.92
36024	77.69 ± 0.98
42060	86.86 ± 1.03
48032	95.70 ± 1.07
53978	104.34 ± 1.10
60013	112.98 ± 1.13
65932	121.32 ± 1.16
71931	129.70 ± 1.19
77913	137.95 ± 1.21
83921	146.18 ± 1.23
90020	154.47 ± 1.25
119990	194.53 ± 1.32
159837	246.72 ± 1.38
199819	298.44 ± 1.43
239738	349.64 ± 1.46
239747	349.60 ± 1.46
319656	451.54 ± 1.51
399593	553.00 ± 1.54
479475	654.12 ± 1.56
559349	755.02 ± 1.57
639367	855.98 ± 1.59
719366	956.82 ± 1.60
799258	1057.49 ± 1.60

(d)$F_{0.9}N_{2.1}$

$H\,(\frac{A}{m})$	$B \pm \sigma_B$ (mT)
0	0.00± < 0.01
5937	16.40 ± 0.27
12008	26.64 ± 0.34
17981	35.57 ± 0.39
24070	44.24 ± 0.42
30043	52.51 ± 0.44
36015	60.62 ± 0.46
42051	68.71 ± 0.47
48023	76.63 ± 0.48
53969	84.46 ± 0.50
59995	92.34 ± 0.50
65914	100.05 ± 0.51
71922	107.85 ± 0.52
77895	115.58 ± 0.53
83903	123.33 ± 0.53
90002	131.17 ± 0.54
119999	169.59 ± 0.56
159828	220.32 ± 0.58
199810	271.05 ± 0.59
239729	321.59 ± 0.6
239747	321.58 ± 0.6
319647	422.57 ± 0.62
399584	523.42 ± 0.63
479475	624.12 ± 0.64
559331	724.71 ± 0.65
639348	825.45 ± 0.66
719348	926.14 ± 0.66
799276	1026.72 ± 0.66

(e)$F_{0.0}N_{6.0}$

$H\,(\frac{A}{m})$	$B \pm \sigma_B$ (mT)
0	0± < 0.01
5901	7.42± < 0.01
11981	15.06± < 0.01
17963	22.58± < 0.01
24052	30.23± < 0.01
30034	37.74± < 0.01
36006	45.25± < 0.01
42051	52.85± < 0.01
48023	60.35± < 0.01
53978	67.84± < 0.01
60004	75.41± < 0.01
65923	82.85± < 0.01
71931	90.40± < 0.01
77913	97.91± < 0.01
83921	105.47± < 0.01
90029	113.14± < 0.01
120008	150.82± < 0.01
159855	200.89± < 0.01
199837	251.14± < 0.01
239756	301.30± < 0.01
239765	301.31± < 0.01
319674	401.74± < 0.01
399611	502.19± < 0.01
479493	602.58± < 0.01
559349	702.93± < 0.01
639366	803.49± < 0.01
719384	904.05± < 0.01
799258	1004.42± < 0.01

(f)$F_{0.0}N_{4.0}$

$H\,(\frac{A}{m})$	$B \pm \sigma_B$ (mT)
0	0.00± < 0.01
5829	7.32± < 0.01
11918	14.97± < 0.01
17909	22.51± < 0.01
23998	30.16± < 0.01
29989	37.69± < 0.01
35997	45.24± < 0.01
42006	52.79± < 0.01
47978	60.29± < 0.01
53933	67.78± < 0.01
59968	75.36± < 0.01
65896	82.81± < 0.01
71895	90.35± < 0.01
77877	97.87± < 0.01
83903	105.44± < 0.01
89993	113.09± < 0.01
119972	150.77± < 0.01
159828	200.86± < 0.01
199819	251.11± < 0.01
239729	301.27± < 0.01
239738	301.27± < 0.01
319638	401.68± < 0.01
399575	502.14± < 0.01
479466	602.54± < 0.01
559331	702.90± < 0.01
639348	803.46± < 0.01
719366	904.02± < 0.01
799258	1004.41± < 0.01

(g)$F_{0.0}N_{3.5}$

$H\,(\frac{A}{m})$	$B \pm \sigma_B$ (mT)
0	0.00± < 0.01
5892	7.40± < 0.01
11972	15.05± < 0.01
17954	22.57± < 0.01
24052	30.23± < 0.01
30025	37.74± < 0.01
35997	45.25± < 0.01
42051	52.86± < 0.01
48014	60.35± < 0.01
53960	67.83± < 0.01
59995	75.41± < 0.01
65923	82.87± < 0.01
71922	90.41± < 0.01
77895	97.91± < 0.01
83930	105.50± < 0.01
90011	113.14± < 0.01
120008	150.85± < 0.01
159855	200.93± < 0.01
199828	251.18± < 0.01
239747	301.36± < 0.01
239747	301.36± < 0.01
319665	401.81± < 0.01
399602	502.29± < 0.01
479484	602.70± < 0.01
559349	703.09± < 0.01
639366	803.67± < 0.01
719402	904.28± < 0.01
799258	1004.65± < 0.01

(h)F_xN_x

$H\,(\frac{A}{m})$	$B \pm \sigma_B$ (mT)
0	0.00± < 0.01
3904	16.31 ± 0.34
7978	33.25 ± 0.70
11990	48.56 ± 1.00
12071	48.78 ± 1.01
24025	80.69 ± 1.51
35979	104.85 ± 1.79
48032	126.53 ± 1.99
59977	146.41 ± 2.13
71922	165.34 ± 2.25
71976	165.25 ± 2.24
108009	218.92 ± 2.50
143826	268.92 ± 2.65
179778	317.48 ± 2.75
215830	365.27 ± 2.82
251737	412.22 ± 2.88
287707	458.89 ± 2.92
323767	505.37 ± 2.96
359710	551.60 ± 2.99
395662	597.53 ± 3.01
799258	1109.87 ± 3.16

through the NHMRC Program Grant 1036078 and ARC Discovery Grant DP120100821.

[1] B. Raaymakers, J. Lagendijk, J. Overweg, J. Kok, A. Raaijmakers, E. Kerkhof, R. van der Put, I. Meijsing, S. Crijns, and F. Benedosso, "Integrating a 1.5 T MRI scanner with a 6 MV accelerator: Proof of concept," *Phys. Med. Biol.*, vol. 54, no. 12, p. N229, 2009.

[2] B. Fallone, M. Carlone, B. Murray, S. Rathee, T. Stanescu, S. Steciw, K. Wachowicz, and C. Kirkby, "Development of a Linac-MRI system for real-time ART," *Med. Phys.*, vol. 34, p. 2547, 2007.

[3] J. Dempsey, D. Benoit, J. Fitzsimmons, A. Haghighat, J. Li, D. Low, S. Mutic, J. Palta, H. Romeijn, and G. Sjoden, "A device for realtime 3D image-guided IMRT," *Int. J. Radiat. Oncol., Biol., Phys., Suppl.*, vol. 63, pp. S202–S202, 2005.

[4] E. Lassner and W.-D. Schubert, *Tungsten: Properties, chemistry, technology of the elements, alloys, and chemical compounds*. Springer, 1999.

[5] B. H. Rabin, A. Bose, and R. M. German, "Characteristics of liquid-phase-sintered tungsten heavy alloys," Tech. Rep., Rensselaer Polytechnic Inst., Troy, NY (USA), 1989.

[6] Midwest Tungsten Service, "Tungsten products", http://www.tungsten.com/

[7] Wolfmet, "Tungsten heavy alloys", http://www.wolfmet.com/

[8] S. Kolling, B. Oborn, and P. Keall, "Impact of the MLC on the MRI field distortion of a prototype MRI-Linac," *Med. Phys.*, vol. 40, no. 12, p. 121705, 2013.

[9] J. D. Jackson, *Classical Electrodynamics Third Edition*. Wiley, third ed., Aug. 1998.

[10] M. Sato and Y. Ishii, "Simple and approximate expressions of demagnetizing factors of uniformly magnetized rectangular rod and cylinder," *J. Appl. Phys.*, vol. 66, no. 2, pp. 983–985, 1989.

[11] Quantum Design USA, "Magnetic property measurement systems", http://www.qdusa.com/sitedocs/productBrochures/1014-003.pdf, 2014

[12] J. J. Bucki, E. Fortuna-Zaleśna, M. Kowalczyk, and Z. Ludyński, "Magnetic properties of tungsten composites," *Kompozyty*, vol. 11, no. 3, pp. 268–273, 2011.

[13] J. J. Bucki, Z. Ludyński, and T. Karwata, "Testing of magnetic properties of tungsten heavy alloys," *Proceedings of European Conference on Advanced Powder Metallurgy Materials*, pp. 347–350, 1995.